THE JOURNAL OF PHYSICAL CHEMISTRY C

pubs.acs.org/JPCC Article

Direct Synthesis of Semimetal Phthalocyanines on a Surface with Insights into Interfacial Properties

Jinbang Hu, Frode Sneve Strand, Rajesh Kumar Chellappan, Zhengde Zhang, Kongchao Shen, Jinping Hu, Gengwu Ji, Ping Huai, Han Huang, Peng Wang, Zheshen Li, Zheng Jiang, Justin W Wells, and Fei Song*

Cite This: J. Phys. Chem. C 2020, 124, 8247−8256 Read Online

ACCESS | Metrics & More | Article Recommendations | Supporting Information

ABSTRACT: On-surface engineering of supramolecular structures has attracted considerable interest during the past few decades. However, organic nanostructures coordinated by group V semimetals have rarely been demonstrated. Herein, we report the metalation of a metal-free phthalocyanine (H_2Pc) via the incorporation of semimetal atoms (Sb and Bi) with insights from X-ray photoelectron spectroscopy, ultraviolet photoelectron spectroscopy, and density functional theory. While H_2Pc becomes completely metalized on the Sb(111) surface after annealing to 200 °C, the metalation of H_2Pc is only partially triggered on Bi(111) at annealing to 300 °C, and the complete metalation is done after further higher temperature annealing. Inspired by the metalation path predicted by DFT calculations, we propose that the metalation of H_2Pc on Sb and Bi semimetals is possible by the dissociation of hydrogen atoms from the pyrrolic nitrogen atom as a result of the orbital hybridization between the N-sp^2 state and the Bi-$6p_y$ state, and the metalation process needs to overcome a relatively high energy barrier due to the weak mixing of atomic orbitals at discriminated energy levels. While Bi/Sb coordinated organic nanostructures have been seldom investigated before, the direct synthesis of SbPc/BiPc via on-surface reaction in this report might bring promising progress for physical chemistry and related fields.

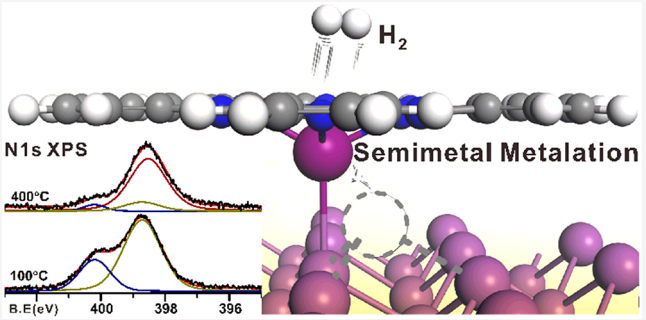

INTRODUCTION

Wide interest has been attracted in past by the on-surface metalation of tetrapyrrole organic layers, namely, porphyrins (Ps), porphyrazines (Pzs). and phthalocyanines (Pcs), due to the promising physiochemical and optoelectronic properties of such metal complexes. In particular, appealing applications have been proposed for metal phthalocyanines (MPcs) in semiconductor devices,[1−4] energy conversion,[5] catalysis,[6−9] and information communication.[10] In addition to this, the coordinated metal atom lying in the center of π-conjugated macrocycles represents well-defined and uniform active sites, thus crediting MPcs with an a giant significance for robust biological and chemical properties.[11−14] Correspondingly, the family of transition metal phthalocyanines (TMPcs) has been synthesized in routine for intense investigation by changing the central coordination atoms,[15] for example, from CuPc to CoPc, FePc, and so on, to find alternative catalysts at low cost toward fuel cells.[14] Nowadays, considerable efforts are still devoted to TMPcs from both experimental and theoretical points of view, in order to exploit novel physiochemical properties for spread applications. For instance, $SnCl_2Pc$ has been proposed for signal transfer between molecules along the predesigned route.[10]

Although numerous investigations have been paid to metallophthalocyanines, interaction between phthalocyanines and nontransitional metal atoms has been scarcely reported.[16] Specifically, Pcs with the group-V atoms coordinated in the center are seldom seen in the literature,[17−19] probably due to the difficulty in synthesizing semimetal organic complexes with nitrogen-donor ligands. On the other hand, such complexes with coordinated semimetals are proposed to have appealing properties in chemistry and biology, such as the effective treatment of diseases, tuning lightfastness and so on.[20] With this motivation, herein, we demonstrate the synthesis of BiPc/SbPc via the metalation of H_2Pc under a dry-chemistry approach, which is performed on group-V semimetal surfaces by external thermal annealing. Sb(111) and Bi(111) are chosen as they are the archetypal semimetal substrates commonly investigated in surface science.[21] The metalation process of H_2Pc on Bi(111) and Sb(111) surfaces is

Received: January 31, 2020
Revised: March 12, 2020
Published: March 16, 2020

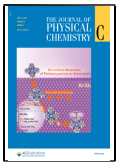

https://dx.doi.org/10.1021/acs.jpcc.0c00895
J. Phys. Chem. C 2020, 124, 8247−8256

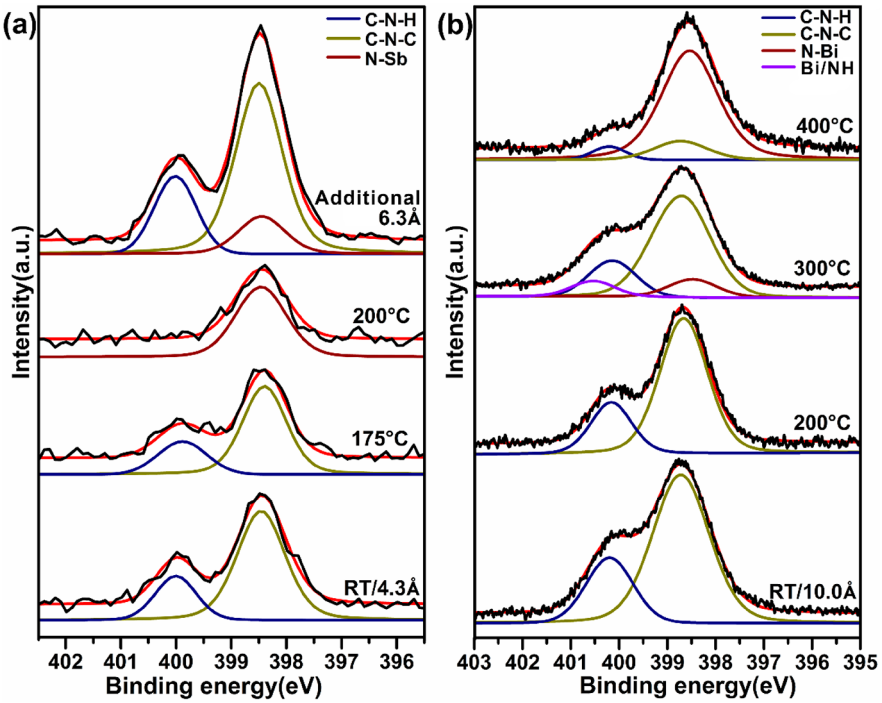

Figure 1. Evolution of N 1s core level spectra of H_2Pc on Sb(111) and Bi(111)/Au as a function of thermal annealing. (a) N 1s spectra recorded after the deposition of 4.3 Å H_2Pc onto Sb(111) at RT followed by thermal annealing to 175 and 200 °C, respectively, and an additional deposition of H_2Pc to multilayer. (b) Changes of N 1s XPS from H_2Pc film (10.0 Å thick) adsorbed on the Bi(111)/Au substrate as a function of in-sequence annealing. Black: raw data. Colored lines: fitted components.

investigated by X-ray photoelectron spectroscopy (XPS) and further supported by density functional theory (DFT) calculations, which predict the reaction path for the on-surface metalation process and identify the electronic structures of as-formed BiPc/SbPc. Moreover, difference of the activation barrier has also been clearly distinguished between the bismuth and antimony atoms involved metalation.

METHODS

Initially, H_2Pc molecules were deposited onto the Sb(111) surface and the bismuth covered Au(111) (where the bismuth film is around 10 nm thick), respectively. As reported in literature, the bismuth film with thickness bigger than seven bilayers usually holds the (111) orientation, since the Bi(111) facet is the preferred growth orientation,[22,23] which has also been confirmed by LEED in the present work. Metal substrates were cleaned by cycles of Ar^+ sputtering and thermal annealing at 500 °C for Au(111) and 200 °C for Sb(111) (Mateck, Germany) under ultrahigh vacuum (UHV), respectively. The quality and cleanliness of crystal surfaces were verified afterward by UPS and XPS. High purity H_2Pc and Bi powder (Sigma-Aldrich, purity higher than 97%) were thoroughly degassed before deposition by heating to a temperature slightly below the sublimation temperature, while the temperature was monitored by a k-type thermocouple close to the evaporator. During deposition, metal substrates were held at room temperature. The bismuth film was annealed at 100 °C for 30 min after deposition onto Au(111) in order to obtain uniform Bi layers. Film thickness was estimated by fitting the peak intensity attenuation from XPS assuming a layer-by-layer growth mode. XPS and UPS measurements of the H_2Pc/Sb(111) absorption system were performed using a PHOIBOS100 electron spectrometer (SPECS GmbH) equipped with a monochromatic Al Kα X-ray source ($h\nu$ = 1486.6 eV) and a helium lamp (He I, $h\nu$ = 21.2 eV) while the base pressure is better than 1×10^{-9} mbar in the UHV chamber.[24] XPS and UPS characterizations of H_2Pc on the Bi(111)/Au surface were performed at the Matline beamline at ISA in Aarhus university, Denmark. Peak fitting of XPS was done using the CASAXPS software.

DFT calculations including the simulation of reaction pathway were carried out in the framework of Perdew–Burke–Ernzerhof (PBE) and generalized gradient approximation (GGA) for the description of the exchange-correlation energy,[25] while projector augmented waves (PAW)[26,27] and a plane wave basis set are implemented in the Vienna ab initio simulation package (VASP). Geometries of the gas-phase metallophthalocyanines and adsorbed systems were fully optimized until the atomic force is smaller than 0.02 eV/Å. An unit cell with dimension of 25 × 25 × 15 $Å^3$ was used for the calculation of gas-phase phthalocyanines, and a slab with three $c(6 \times 6)$ layers of semimetal atoms and the vacuum thickness of 19.0 Å was utilized to simulate the adsorption complex, while the bottom two semimetal layers were kept frozen during optimization. The energy cutoff was set to 500 eV for the plane wave set. A 2 × 2 × 1 Monkhorst–Pack k-point mesh was used. Charge densities for the adsorption configuration were plotted on the basis of Bader analysis. The prediction of the metalation reaction for H_2Pc on Sb(111) and Bi(111) was performed by the climbing-image (CI) NEB modified method.[28]

RESULTS AND DISCUSSION

To check whether the metalation of H_2Pc can happen on Sb(111), the change of N 1s core level from XPS after adsorption is an evidence fingerprint, as widely discussed in

https://dx.doi.org/10.1021/acs.jpcc.0c00895
J. Phys. Chem. C 2020, 124, 8247–8256

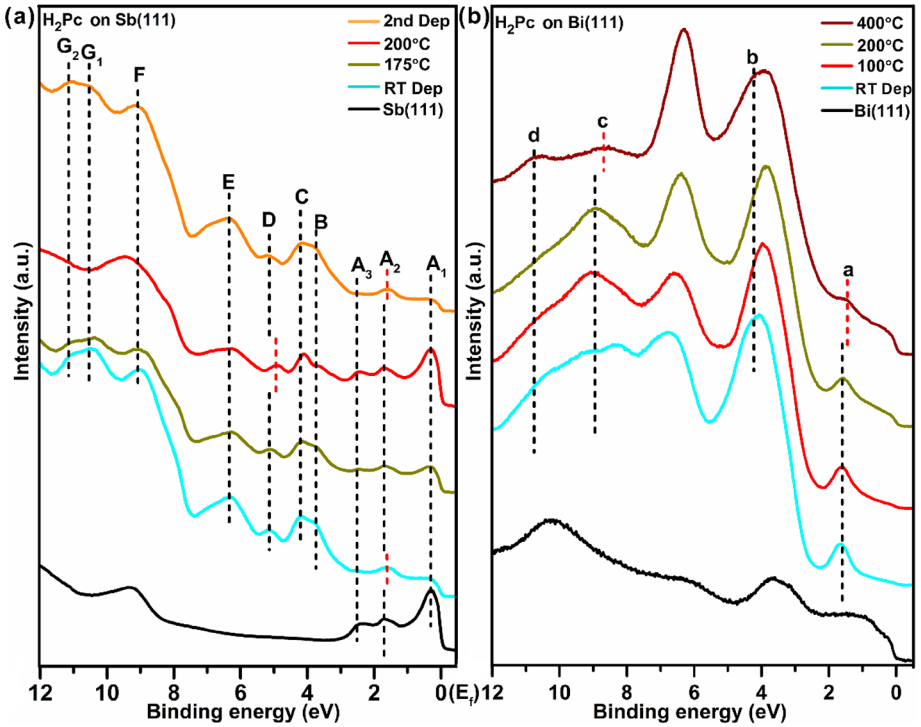

Figure 2. Evolution of valence band spectra of (a) the H_2Pc/Sb(111) system and (b) H_2Pc on Bi(111) surface at sequential annealing steps.

previous reports.[29] Initial deposition of 4.3 Å H_2Pc on Sb(111) was performed followed by stepwise annealing, while in situ XPS measurements were done to monitor chemical state changes of the nitrogen atom, as shown in Figure 1a. It can be judged from the molecular structure that H_2Pc comprises two chemically different types of nitrogen atoms: the pyrrolic (−NH−, denoted as N_P in this paper) and the iminic (=N−) nitrogen (denoted as N_I). It is obvious in Figure 1a that, the N 1s spectrum of as-deposited H_2Pc on the Sb(111) surface at RT indeed own two components. The peak located at 400.0 eV should be assigned to the N_P atom, while the component staying at 398.5 eV originates from the N_I atom, as compared to literature reports.[29,30] Similarly, in the case of 10.0 Å H_2Pc on Bi(111)/Au at RT, there are also two components with the binding energy at 400.2 and 398.7 eV, respectively, which are supposed to origin from the N_P and N_I atoms as well. Moreover, the peak intensity ratio between these two components is found to be 1:2.97 for H_2Pc on Sb(111) and 1:3.03 for H_2Pc on the Bi(111) surface, corresponding well to the molecular stoichiometry of 1:3.

Following the initial deposition of H_2Pc on Sb(111) and Bi(111), thermal annealing was performed afterward in sequence. At the first stage, no visible change is observed in the line shape of the N 1s spectrum after annealing to 175 °C for the H_2Pc/Sb(111) system or after annealing to 200 °C in the case of H_2Pc/Bi(111). Specifically, both the peak position and intensity ratio of these two components remain unchanged, indicating that no reaction occurs at interface at this stage. Interestingly, further annealing the H_2Pc/Sb(111) system to 200 °C leads to dramatic changes. The N 1s component located at 400.0 eV originating from N_P atoms completely disappears while the peak at 398.5 eV remains in the spectrum. Such change clearly indicates that nitrogen atoms of phthalocyanines are now faced to a new chemical environment. Disappearance of the N_P component suggests that the original −NH− group no longer exists and that the pristine pyrrolic nitrogen might get coupled to the Sb atom as compared to XPS spectra in the metalation of H_2Pc on Cu(111) or other transition metal (TM) surfaces.[29,31] On the other hand, since there is only one relatively broad peak resolved in the N 1s spectrum after annealing to 200 °C, it can be speculated that the Sb-bonded N atoms might have a similar binding energy as the iminic nitrogen. In practice, analogous phenomena have been reported in literature, for example, the N 1s spectrum from CoPc and CuPc was revealed to have only one component including both the metal-coordinated and iminic nitrogen atoms,[15,29] which therefore makes it difficult to distinguish them from XPS. To make the metalation demonstration convincing, an additional deposition of H_2Pc (around 6.3 Å more) to multilayer coverage was done, which results in the emergence of the pristine N_P component and therefore supports the metalation of H_2Pc at interface.

The occurrence of metalation of H_2Pc with semimetal is further confirmed by recording the evolution of the N 1s core level from an analogous system with 10 Å thick H_2Pc on Bi(111) as a function of thermal annealing, as depicted in Figure 1b. It can be resolved that the N_P component gradually becomes broad when annealing from RT to 300 °C, probably indicating the occurrence of partial reaction in the H_2Pc/Bi(111) complex was induced at 300 °C annealing. Interestingly, besides the pristine N_P and N_I components, one additional peak has to be introduced in the N 1s spectrum to obtain reasonable fitting in Figure 1b, which is revealed to be at the binding energy of 400.5 eV. Since the metal coordinated nitrogen and iminic nitrogen in phthalocyanines are very close to each other in XPS (398.5 and 398.7 eV, respectively obtained from fitting), we propose that the new component at 400.5 eV might be assigned to the Bi coordinated or bound pyrrolic. Moreover, the peak intensity ratio between the component at 400.2 eV (N_P) and at 398.7

https://dx.doi.org/10.1021/acs.jpcc.0c00895
J. Phys. Chem. C 2020, 124, 8247−8256

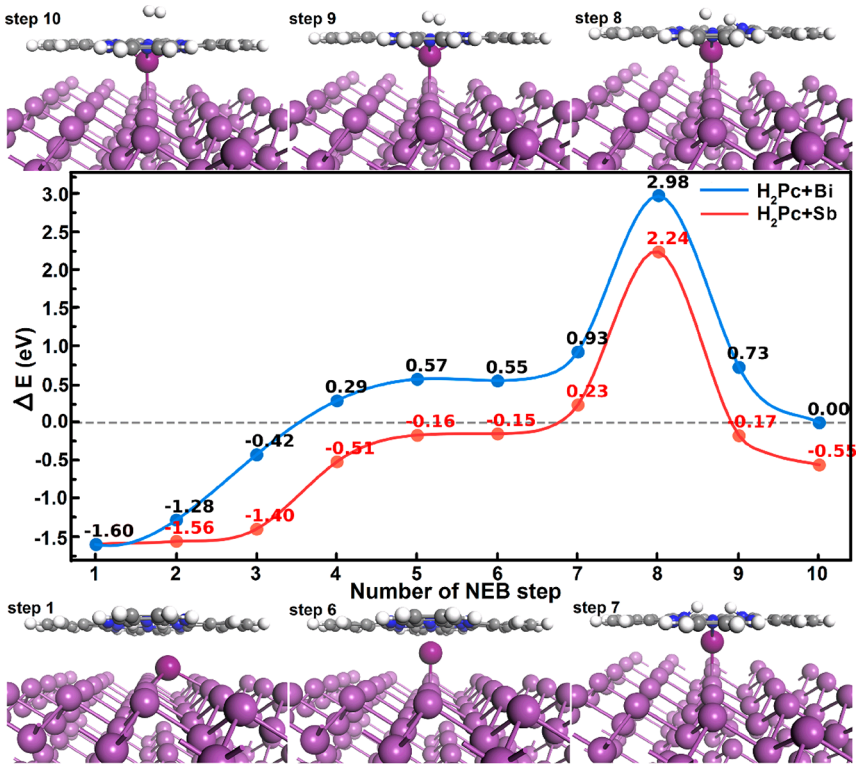

Figure 3. NEB predicted path for the metalation reaction of H_2Pc with a Bi atom on Bi(111) (blue) and H_2Pc with a Sb atom on Sb(111) (red). Intermediate states in the metalation procedure are shown and labeled with the relative energy barrier compared to the final step with the BiPc and H_2 products. Pink: bismuth. Dark gray, carbon. Blue, nitrogen. White, hydrogen.

eV (N_I) is now analyzed to be 3.95, which is apparently lower compared to the initial value at RT, pointing out the decline of N_P component. Further annealing to 400 °C, the N_P component is significantly reduced but not completely gone, which could be derived from unreacted H_2Pc molecules from multilayer.[32,33] In fact, the analogous macrocycle of 2*H*-tetraphenylporphyrin on the iron-decorating Ag(111) surface also shows the pyrrolic component coexists with the Fe(II)−tetraphenylporphyrin feature after annealing to 550 K.[34] Therefore, it can be judged that the metalation of H_2Pc on Bi(111) is temperature-dependent, similar to the metalation of H_2Pc on Cu(111).[29] Based on these results, we can conclude that the metalation of H_2Pc on the Bi(111) surface starts from around 300 °C and is most probably completed at 400 °C annealing. Compared to the metalation of H_2Pc on Sb(111), which is finished after annealing to 200 °C, a relatively high thermal energy is needed to trigger the metalized reaction of H_2Pc on Bi(111), which also suggests that the metalation activity or catalytic ability of antimony to the H_2Pc macrocycle is stronger than that of bismuth in the framework of on-surface reaction.

To shed more insights on the metalation of H_2Pc with Sb and Bi, ultraviolet photoemission spectroscopy (UPS) was performed to exploit valence band structures during the metalation procedure and is depicted in Figure 2. As expected for the H_2Pc on Sb(111), there are several new features appearing in the binding energy range 0 to 12 eV in Figure 2a (labeled as B−G) while the surface state is found to be at a binding energy of around 0.4 eV (marked as A_1) below the Fermi level (E_f). Valence structures at 1.8 and 2.6 eV derived from the Sb 5p state of the clean Sb(111) get quenched after the adsorption of H_2Pc at RT as seen in Figure 2a. Additionally, the component of A_2 can be assigned to the highest occupied molecular orbital (HOMO) level of H_2Pc on Sb(111). Subsequently heating to 175 °C partially recovers the valence structures, while peaks B−G at higher binding energy becomes weak with slight difference in energy due to the desorption of molecules. Interestingly, further annealing to 200 °C results in obvious changes of valence structures. First, peak B located at 3.6 eV becomes weak while peak C at 4.2 eV gets sharp and more dominant with a slight shift toward lower binding energy, and the similar shift goes with peak D as well. Moreover, peak F located at 9.0 eV moves toward larger binding energy and another two peaks labeled as G_1 and G_2 completely disappear. Since additional deposition of H_2Pc brings pristine features from H_2Pc molecules back, we therefore infer these obvious changes of interface electronic structure at 200 °C result from new adsorbates formed on Sb(111), which was also confirmed in the XPS results. As compared to the situation of annealing at 175 °C, the peak near the right side of peak C, and the lower binding energy peak beside peak D and the larger binding energy peak near peak F appear after heating to 200 °C should be attributed to the mixing between atomic orbitals within the inner iminic N (in the pentagon of porphyrin compared to other iminic N atoms at the corner of porphyrin) and Sb valence states. On the other hand, the fading of features G_1, G_2 and the weakening of peak B might also be related to the removal of adsorbed H_2Pc on Sb(111). Notably, there is a wide peak clearly visible around 4.0 eV below E_f (labeled as E) which remains constant and could be assigned to the Pc macrocycle, mainly the π-conjugated MOs formed by sp^2 hybrid state between carbon and nitrogen atoms, since these MOs can hardly be influenced.[28]

https://dx.doi.org/10.1021/acs.jpcc.0c00895
J. Phys. Chem. C 2020, 124, 8247−8256

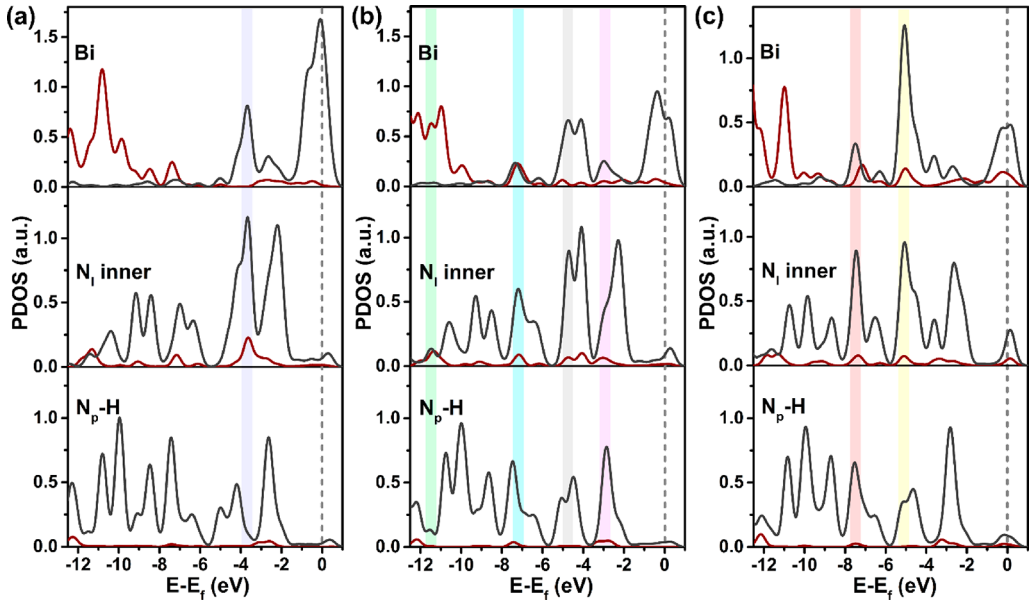

Figure 4. Partial density of states (PDOSs) on Bi, iminic N_I and pyrrolic N_P atoms are calculated to exploit the evolution of orbital hybridization among reaction steps 6, 7, and 8. (a) Hybridized state labeled with violet bar between the Bi and inner N_I atoms in step 6. (b) Four new mixed states between Bi and N_P atoms in step 7 and (c) another two coupled MOs in step 8. Red: s state. Gray: p state.

Moreover, obvious changes of interfacial electronic structures have also been found in the H_2Pc/Bi(111) adsorption system after heating to 400 °C (Figure 2b), which might be seen as an indicator of the surface mediated process for H_2Pc on Bi(111). Specifically, the HOMO from H_2Pc is clearly resolved at around 1.6 eV (marked as "a") below E_f after deposition onto the Bi thin film at RT. Subsequently, peak "a" moves toward to the Fermi level side when heating to 400 °C, which may result from the interfacial charge transfer from Bi atoms to the H_2Pc macrocycle. Meanwhile, a new structure appears at the binding energy of 4.2 eV below E_f, which is similar to the feature C observed in the H_2Pc/Sb(111) system. Contrary to the shift to larger binding energy of peak F and the disappearance of peak G_1 and G_2 after metalation in the H_2Pc/Sb(111) system, annealing the H_2Pc/Bi(111) system to 400 °C results in the shift of peak "c" to lower binding energy while a new feature labeled as "d" formed, respectively. It can therefore be inferred the interfacial electronic structures of H_2Pc/Bi(111) adsorption system has been modified after heating to 400 °C due to the orbital coupling between bismuth valence states and molecular orbitals contributed by the pyrrole. In a word, changes of interfacial electronic structures have been indeed discovered for H_2Pc adsorbed on Sb(111) after annealing to 200 °C and on Bi(111) at annealing to 400 °C, agreeing reasonably with previous discussions of XPS results, while both UPS and XPS results suggest together that H_2Pc can be metalized by Sb and Bi semimetals after thermal annealing. Last but not least, it needs to be addressed that changes of valence structures for the metalation of H_2Pc are quite similar on both Sb(111) and Bi(111) substrates, although rich features are observed initially in the UPS of the pristine Sb(111) compared to the Bi(111) surface, as bismuth has relatively low density of states around Fermi level.[38]

Photoemission spectroscopy results demonstrate the metalation of H_2Pc on both Sb(111) and Bi(111) semimetal substrates, we have performed DFT calculations with the nudged elastic band (NEB) method to get a further insight into the metalation procedure of H_2Pc on both the bismuth and antimony surfaces. Reactants are set to be H_2Pc and one Bi or Sb atom on top of the Bi(111) or Sb(111) surface, while the products are a metalized macrocycle of BiPc or SbPc and H_2 gas. As the reaction mechanism is revealed to be similar on both substrates as depicted in Figure 3, where the reaction on Sb(111) is marked with red and blue on Bi(111), only one metallization procedure is chosen and discussed in detail as an example: H_2Pc on Bi(111). Based on the assumption that surface atoms can be induced by thermal annealing, a Bi atom was first placed at the hollow site on top of three bismuth layers, and it can move freely around surface during reaction. The predicted metalation path is summarized in Figure 3, and it can be seen that the Bi adatom moves from the initial hollow site to the top site (from step 1 to step 6) and stays exactly underneath the center of H_2Pc. Afterward, the Bi atom is lifted up and jumps into the H_2Pc macrocycle being bonded to two N_P atoms to form a H_2Pc−Bi intermediate state (step 7). As the on-surface reaction continues, one N−H bond is first activated by and bound sequentially to the Bi atom. When it goes further to the highest barrier step (step 8), the second hydrogen atom isdissociated from the N_P atom as well. Ultimately, the BiPc macrocycle is formed by desorbing two leased hydrogen atoms in the form of H_2. As revealed from the reaction diagram, the highest energy barrier to overcome during the metalation procedure is 2.43 eV from step 6 (0.55 eV) to step 8 (2.98 eV), which is in general consistent with our experimental observation according to the Arrhenius equation, and it is apparently higher than the metalation of H_2Pc by Zn, Fe, V, Co, or other metal atoms,[36,37] Since bismuth is relatively inert compared to other transition metals and has a low density of states close to Fermi level,[38] it therefore makes sense that the metalation of H_2Pc with Bi involves a higher activation energy by relatively intense thermal annealing up to 400 °C which is close to the melting point of the bismuth crystal but still far below that of the Bi(111)/Au system. The procedure is endothermic in total with the energy of 1.6 eV required, which

https://dx.doi.org/10.1021/acs.jpcc.0c00895
J. Phys. Chem. C 2020, 124, 8247−8256

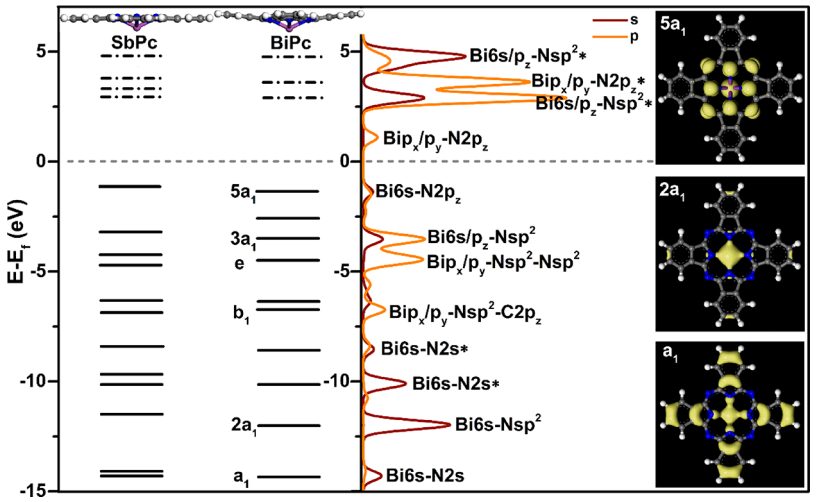

Figure 5. Energy level diagram of MOs from the gas-phase BiPc/SbPc labeled by the C_{4v} irreducible representation, and the corresponding contribution to the PDOS of BiPc identified as an example. For easy discussion, three typical MOs from BiPc under the C_{4v} constraint, a1, 2a1, and 5a1 with the isovalue of ±0.005, ± 0.02, and ±0.01 e/bohr^3, respectively, are also shown on the right side. * indicates antibonding.

indicates that the metalation of H_2Pc on bismuth cannot be triggered easily.

Derived from the predicted reaction path, electronic properties of intermediate states have also been investigated to clarify the metalation mechanism of the N−H bonding activated by the semimetal atom. As judged from the partial density of state (PDOS) from the Bi atom, the N_I and N_P atoms in step 6 shown in Figure 4a, there are several hybridized states between the bismuth atom and its neighbors via valence states mixing. Interestingly, the hybridization is found between the Bi $6p_z$ and N_I sp^2 states to form the Bi $6p_z$−N_I sp^2 intermediate state in step 6 as highlighted Figure 4a, while the corresponding MO configuration is shown in Figure S2a. It can be inferred that, additional activation energy could enhance the orbital mixing between H_2Pc MOs and valence states of Bi atom, subsequently leading to new mixed states in step 7, beside the Bi $6p_z$−N_I sp^2 state already shown in step 6 which now moves to −4.2 eV at this reaction step. These new mixings are revealed to be couplings between the Bi and N_I atoms and the relatively weak coupling between Bi and N_P atoms, respectively. Deep investigation shows that these new hybridized states (as depicted in Figure 4b) are the Bi 6s−N_I sp^2 state at −11.5 eV, Bi $6p_x$−N_Ip_z at −7.3 eV, Bi $6p_x$−N_I sp^2 at −4.7 eV which contribute to the formation of Bi−N_I bonding, and the MO at −2.9 eV from the coupling between Bi $6p_y$ and N_P sp^2 states which indicates that the N_P−H bond starts to be activated by Bi, in respond to the additionally introduced N 1s component in Figure 1b at a binding energy of 400.5 eV. Detailed information can also be found in Figure S2b in the Supporting Information.

Further to the top barrier with step 8 in Figure 4c, the MO at −5.1 eV (also shown in Figure S2b) is the mixing state of Bi $6p_y$-N_Psp^2-H with major contribution from the Bi $6p_y$ state. Meanwhile, another MO at −7.6 eV is originated from the hybridization between Bi and N_P with the coupling style of Bi $6p_y$−N_P p_z, stating that the Bi $6p_y$ state is ready to activate the N_P−H bonding. Therefore, we can propose that the Bi $6p_y$ state plays an important role in activation of the N_P−H bond. In addition, as seen from the PDOS of both Bi and N_P atoms in step 6, the relatively poor mixing between the Bi $6p_y$ and valence states of N atoms requires higher thermal energy to trigger the metalation reaction of H_2Pc compared to that on other TM substrates, where 3d orbitals of TM atoms can couple relatively easily with the valence states of the N_P and H atoms due to the proximity of energy levels of MOs and the orbital configuration of d_{xz} and d_{yz} states.

As the metalation mechanism of H_2Pc on Bi(111) has been exploited in detail, we now move the focus to the metalized macrocycles. It has been reported that molecular structures of TMPc in gas-phase are inclined to have the D_{4h} symmetry;[35] however, both SbPc and BiPc are revealed to possess the C_{4v} symmetry after full optimization as shown in Figure 5, where the central semimetal atom is lifted outside the Pc plane. Calculations based on the gas-phase configuration shows that varied hybridized orbitals could be induced via couplings between the Bi 6s/6p states (Sb 5s/5p states) and the 2s/2p states of N_I atoms. In corresponding to PDOS, MOs of the gas-phase BiPc and SbPc are shown for direct comparison. By comparing the PDOS of N_I and Bi from the gas-phase BiPc as shown in Figure S3 in the Supporting Information, we can also propose the coupling manner between the Bi and N valence states: under the strong plane field induced by the Pc macrocycle, p states of the Bi(Sb) ion split into A1(p_z) and E(p_x, p_y) levels. According to the hybridization of MOs and orbital configurations listed in Figure 5 with three typical MOs shown on the right (a1, 2a1, and 5a1), it is inferred that the Bi valence states are mixed mainly with three types of N valence states: 2s, p_z, and sp^2. It shall be addressed that both the doubly degenerated b1 and e MOs appear with the same hybridization form: the $6p_x$ or $6p_y$ state of Bi mixing with the sp^2 hybrid sate of N_I (Bi $6p_x/p_y$−N sp^2). In conclusion, hybridized states between valence states of semimetal and N_I atoms shed convincing insights on forming the stable Bi−N_I or Sb−N_I bonding under the C_{4v} symmetry constraint.

Besides the discovery of C_{4v} symmetry in BiPc, it might also be meaningful to exploit interfacial electronic properties in the adsorption configuration of SbPc (BiPc) on Sb(111) (Bi(111)), which stands for a new type of interface with the organo-semimetallic adsorption on semimetal. In the case of the TMPcs' adsorption on metal substrates, molecules are usually arranged with their aromatic plane parallel to the substrate.[35] In practice, the adsorption configuration of Pcs on

https://dx.doi.org/10.1021/acs.jpcc.0c00895
J. Phys. Chem. C 2020, 124, 8247−8256

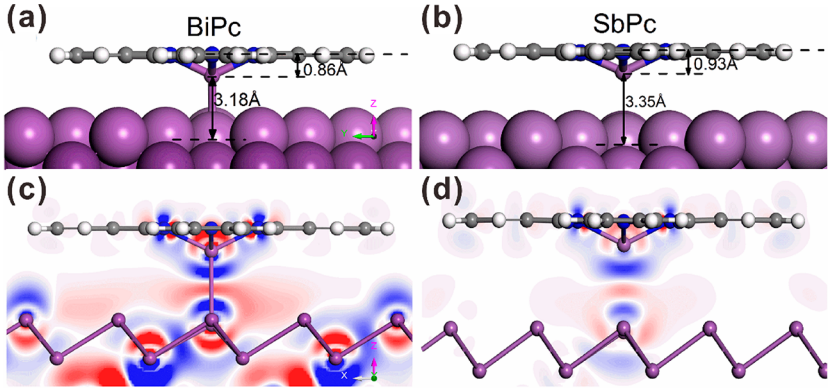

Figure 6. Adsorption geometry of (a) BiPc on Bi(111) and (b) SbPc on Sb(111). Corresponding charge density differences are plotted in parts c and d, respectively, with the isovalue of 0.01 e/bohr^3.

varying substrates is affected by several parameters, for example, the adsorption site, the azimuthal orientation of the macrocycle with respect to substrate and the adsorption height.[39] Similar to the report of SnPc on Ag(111),[40] geometry optimization herein also shows that an apparent distortion of the molecular plane is induced when BiPc is placed on top of Bi(111), while a similar distortion is also found for the adsorption of SbPc on Sb(111), as shown in Figure 6. It can also be discovered that BiPc is, in principle, chemically adsorbed on the Bi(111) surface with the central Bi ion anchored to substrate and a Bi−Bi bonding length of 3.18 Å is revealed along the surface normal direction with the molecular plane placed 4.04 Å above the bismuth substrate. On the other hand, the binding of SbPc on Sb(111) is slightly different: the distance from the central Sb atom of SbPc to substrate is 3.35 Å with no obvious chemical bonding formed, and the Pc plane is arranged with the adsorption height of 4.28 Å. These results suggest that the adsorption of SbPc on Sb(111) might be governed by weak molecule−substrate interactions while BiPc is chemically ad sorbed on Bi(111). Moreover, the Bi−N bonding length for adsorbed MPcs is also considered and summarized in Table S1 in the Supporting Information, while a length of 2.19 and 2.25 Å are found for SbPc and BiPc, respectively, as compared to the length of 2.17 and 2.28 Å in the gas phase.

Moreover, investigation of charge redistribution upon adsorption might also be helpful to understand the adsorption mechanism. The charge density difference induced by the adsorption is defined as $\Delta\rho = \rho_{tot} - \rho_{sub} - \rho_{mol}$, where ρ_{tot} is the charge density of the adsorption system, and ρ_{sub} and ρ_{mol} and the charge density of the clean Sb(111) and Bi(111) substrate and the gas-phase SbPc or BiPc, respectively. As judged from Figure 6, where the red color represents charge accumulation and blue denotes charge depletion, it is obvious that the charge redistribution at the BiPc/Bi(111) interface is much more apparent than that at the SbPc/Sb(111) system, supporting the previous discussion that the BiPc molecule is chemically adsorbed on the Bi(111) surface while SbPc is relatively weakly attracted by the Sb(111) substrate. Furthermore, the inner N atom in the adsorbed BiPc shows a higher charge accumulation as compared to that in the adsorbed SbPc, indicating that the coordinated Bi atom could have a stronger influence on the chemical environment of the inner N atom than that in the SbPc/Sb(111) system. This difference is also in agreement with changes in N 1s core level spectra, where a shift of N 1s with about 0.2 eV is observed on Bi(111) after heating to 400 °C while no obvious shift was found on the Sb(111) substrate. For a detailed understanding of the charge transfer at the BiPc/Bi(111) interface, a comparison between the gas-phase BiPc and the adsorbed BiPc on Bi(111) has also been performed and presented in Figure S4 in the Supporting Information.

In a word, the metalation of H_2Pc on both Sb and Bi semimetal substrates have been proposed by XPS and UPS discussion, and further verified by NEB and DFT calculations. While the metalation of H_2Pc on other transition metal surfaces have been widely reported in literature, herein, the demonstration of on-surface synthesis of semimetal phthalocyanines on Sb and Bi substrates might shed interesting insights onto the on-surface physics and chemistry for further exploiting of phthalocyanines. While the mechanism of on-surface metalation of H_2Pc by semimetals has been investigated, the feasibility of metallizing H_2Pc by the Sb/Bi atom is proven with the SbPc molecule to be formed much easier than BiPc due to the relatively high activity of Sb. Moreover, it is discovered that the synthesized BiPc is strongly adsorbed on the bismuth substrate while SbPc is physically attracted on top of the Sb surface, which might also point out an effective approach for interfacial engineering of semimetallic organics toward molecular electronics in future.

CONCLUSIONS

On-surface metalation of H_2Pc on both the Sb(111) and Bi(111) semimetal substrates has been demonstrated herein by XPS measurements and DFT calculations, and a systematic investigation of the reaction mechanism on both surfaces has been carried out. Regarding on the formation of BiPc, XPS shows that the metalation of H_2Pc with Bi atoms starts to occur with annealing at 300 °C, and the reaction is further promoted and finished after subsequent annealing to 400 °C. On the other hand, the metalation reaction of H_2Pc on Sb(111) is revealed to be completely finished after annealing to 200 °C. With additional insights from DFT calculations, it is found that the metalation of H_2Pc with Bi is endothermic with an external energy required (1.60 eV), while the formation of SbPc on Sb(111) is exothermic with energy released (1.23 eV). As judged from the summarized reaction diagram, the highest activation energy to overcome toward the formation of BiPc is 2.43 eV, which is a bit higher than the situation of SbPc with 2.39 eV, in good agreement with the discussion of XPS results. Moreover, BiPc is found to be chemically adsorbed on Bi(111) while SbPc is weakly attracted by Sb(111). It is therefore

https://dx.doi.org/10.1021/acs.jpcc.0c00895
J. Phys. Chem. C 2020, 124, 8247−8256

concluded from DFT predictions that the metalation of H_2Pc is associated with the hybridization between valence states of the bismuth and neighboring nitrogen atoms, while the 6p state of Bi plays an important role in mixing with the inner N_I to produce the intermediate complex BiH_2Pc and subsequently the dehydrogenation of N_P atoms. The metalation process needs to overcome a considerable energy barrier due to the fact that the valence states of Bi or Sb are located higher than the N_P sp^2−H 1s state resulting in relatively weak orbital hybridization. Encouragingly, the direct synthesis of SbPc and BiPc via the on-surface approach herein might highlight an appealing approach toward the fabrication of semimetal coordinated macrocycles and nanostructures using the dry-chemistry concept, and it possesses appealing potentials in the field of physics, chemistry and materials sciences.

■ ASSOCIATED CONTENT

Supporting Information

The Supporting Information is available free of charge at https://pubs.acs.org/doi/10.1021/acs.jpcc.0c00895.

XPS of the Bi 5d core level from substrate during the sequential annealing, hybridized MOs in steps 6, 7, and 8 of the metalation procedure of H_2Pc/Bi(111), comparison of the gas-phase BiPc and adsorbed BiPc in the point view of MOs, and PDOS and key parameters of semimetal Pcs in gas-phase and adsorption configuration (PDF)

■ AUTHOR INFORMATION

Corresponding Author

Fei Song − *Key Laboratory of Interfacial Physics and Technology, Shanghai Institute of Applied Physics, Shanghai 201204, China; University of Chinese Academy Sciences, 101000 Beijing, China; Shanghai Synchrotron Radiation Facility, Zhangjiang Lab, Shanghai Advanced Research Institute, Chinese Academy of Sciences, Shanghai 201204, China;* orcid.org/0000-0002-6408-7796; Email: songfei@sinap.ac.cn

Authors

Jinbang Hu − *Key Laboratory of Interfacial Physics and Technology, Shanghai Institute of Applied Physics, Shanghai 201204, China; University of Chinese Academy Sciences, 101000 Beijing, China; Center of Quantum Spintronics and Department of Physics, Norwegian University of Science and Technology, Trondheim, NO 7491, Norway*

Frode Sneve Strand − *Center of Quantum Spintronics and Department of Physics, Norwegian University of Science and Technology, Trondheim, NO 7491, Norway*

Rajesh Kumar Chellappan − *Center of Quantum Spintronics and Department of Physics, Norwegian University of Science and Technology, Trondheim, NO 7491, Norway*

Zhengde Zhang − *Key Laboratory of Interfacial Physics and Technology, Shanghai Institute of Applied Physics, Shanghai 201204, China*

Kongchao Shen − *Key Laboratory of Interfacial Physics and Technology, Shanghai Institute of Applied Physics, Shanghai 201204, China; Shanghai Synchrotron Radiation Facility, Zhangjiang Lab, Shanghai Advanced Research Institute, Chinese Academy of Sciences, Shanghai 201204, China*

Jinping Hu − *Key Laboratory of Interfacial Physics and Technology, Shanghai Institute of Applied Physics, Shanghai 201204, China; Shanghai Synchrotron Radiation Facility, Zhangjiang Lab, Shanghai Advanced Research Institute, Chinese Academy of Sciences, Shanghai 201204, China*

Gengwu Ji − *Key Laboratory of Interfacial Physics and Technology, Shanghai Institute of Applied Physics, Shanghai 201204, China*

Ping Huai − *Key Laboratory of Interfacial Physics and Technology, Shanghai Institute of Applied Physics, Shanghai 201204, China; University of Chinese Academy Sciences, 101000 Beijing, China*

Han Huang − *School of Physics Science and Electronics, Central South University, Changsha 410083, China;* orcid.org/0000-0003-0641-1962

Peng Wang − *Department of Applied Physics, College of Electronic and Information Engineering, Shandong University of Science and Technology, Qingdao 266590, China*

Zheshen Li − *Institute for Storage Ring Facilities (ISA), Department of Physics and Astronomy, Aarhus University, 8000 C Aarhus, Denmark*

Zheng Jiang − *Key Laboratory of Interfacial Physics and Technology, Shanghai Institute of Applied Physics, Shanghai 201204, China; University of Chinese Academy Sciences, 101000 Beijing, China; Shanghai Synchrotron Radiation Facility, Zhangjiang Lab, Shanghai Advanced Research Institute, Chinese Academy of Sciences, Shanghai 201204, China;* orcid.org/0000-0002-0132-0319

Justin W Wells − *Center of Quantum Spintronics and Department of Physics, Norwegian University of Science and Technology, Trondheim, NO 7491, Norway;* orcid.org/0000-0001-6366-366X

Complete contact information is available at: https://pubs.acs.org/10.1021/acs.jpcc.0c00895

Author Contributions

The manuscript was written through contributions of all authors. All authors have given approval to the final version of the manuscript.

Notes

The authors declare no competing financial interest.

■ ACKNOWLEDGMENTS

Fruitful discussions with Prof. Dr. Q. Chen and Dr. Yaobo Huang are greatly appreciated. This work is financially supported by The National Key Research and Development Program of China (2016YFA0401302), National Natural Science Foundation of China (11874380, 11874427, U1732267), and the Hundred Talents Program of the Chinese Academy of Sciences. This work is also supported by the Research Council of Norway through its Centres of Excellence funding scheme, Project Number 262633, "QuSpin".

■ REFERENCES

(1) Liu, J.; Li, C.; Liu, X. Q.; Lu, Y.; Xiang, F. F.; Qiao, X. L.; Cai, Y. X.; Wang, Z. P.; Liu, S. Q.; Wang, L. Positioning and Switching Phthalocyanine Molecules on a Cu(100) Surface at Room Temperature. *ACS Nano* **2014**, *8*, 12734−12740.

(2) Song, F.; Wells, J. W.; Handrup, K.; Li, Z. S.; Bao, S. N.; Schulte, K.; Ahola-Tuomi, M.; Mayor, L. C.; Swarbrick, J. C.; Perkins, E. W.; et al. Direct Measurement of Electrical Conductance through a Self-assembled Molecular Layer. *Nat. Nanotechnol.* **2009**, *4*, 373−376.

(3) Melville, O. A.; Grant, T. M.; Lessard, B. H. Silicon Phthalocyanines as N-type Semiconductors in Organic Thin Film Transistors. *J. Mater. Chem. C* **2018**, *6*, 5482−5488.

(4) Ozaki, M.; Yoneya, M.; Shimizu, Y.; Fujii, A. Carrier Transport and Device Applications of The Organic Semiconductor Based on Liquid Crystalline Non-peripheral Octaalkyl Phthalocyanine. *Liq. Cryst.* **2018**, *45*, 2376−2389.
(5) Barth, J. V.; Costantini, G.; Kern, K. Engineering Atomic and Molecular Nanostructures at Surfaces. *Nature* **2005**, *437*, 671−679.
(6) Zhang, C. Z.; Hao, R.; Yin, H.; Liu, F.; Hou, Y. L. Iron Phthalocyanine and Nitrogen-doped Graphene Composite as a Novel Non-precious Catalyst for The Oxygen Reduction Reaction. *Nanoscale* **2012**, *4*, 7326−7329.
(7) Sedona, F.; Di Marino, M.; Forrer, D.; Vittadini, A.; Casarin, M.; Cossaro, A.; Floreano, L.; Verdini, A.; Sambi, M. Tuning The Catalytic Activity of Ag(110)-supported Fe Phthalocyanine in the Oxygen Reduction Reaction. *Nat. Mater.* **2012**, *11*, 970−977.
(8) Hulsken, B.; Van Hameren, R.; Gerritsen, J. W.; Khoury, T.; Thordarson, P.; Crossley, M. J.; Rowan, A. E.; Nolte, R. J. M.; Elemans, J. A. A. W.; Speller, S. Real-time Single-molecule Imaging of Oxidation Catalysis at a Liquid-solid Interface. *Nat. Nanotechnol.* **2007**, *2*, 285−289.
(9) Jiang, Y. Y.; Lu, Y. Z.; Lv, X. Y.; Han, D. X.; Zhang, Q. X.; Niu, L.; Chen, W. Enhanced Catalytic Performance of Pt-Free Iron Phthalocyanine by Graphene Support for Efficient Oxygen Reduction Reaction. *ACS Catal.* **2013**, *3*, 1263−1271.
(10) Li, C.; Wang, Z. P.; Lu, Y.; Liu, X. Q.; Wang, L. Conformation-based Signal Transfer and Processing at the Single-molecule Level. *Nat. Nanotechnol.* **2017**, *12*, 1071−1076.
(11) Bräuer, B.; Vaynzof, Y.; Zhao, W.; Kahn, A.; Li, W.; Zahn, D. R. T.; Fernández, C. J.; Sangregorio, C.; Salvan, G. Electronic and Magnetic Properties of Ni Nanoparticles Embedded in Various Organic Semiconductor Matrices. *J. Phys. Chem. B* **2009**, *113*, 4565−4570.
(12) Kamau, G. N.; Rusling, J. F. Enhanced Rates of Organic Dehalogenations in a Microemulsion Using Adsorbed Metal Phthalocyanines on Electrodes. *Langmuir* **1996**, *12*, 2645−2649.
(13) Aguirre, M. J.; Isaacs, M.; Armijo, F.; Basáez, L.; Zagal, J. H. Effect of the Substituents on the Ligand of Iron Phthalocyanines Adsorbed on Graphite Electrodes on Their Activity for the Electrooxidation of 2-Mercaptoethanol. *Electroanalysis* **2002**, *14*, 356−362.
(14) Shui, J. L.; Wang, M.; Du, F.; Dai, L. M. N-doped Carbon Nanomaterials Are Durable Catalysts for Oxygen Reduction Reaction in Acidic Fuel Cells. *Science. Adv.* **2015**, *1*, No. e1400129.
(15) Shen, K. C.; Narsu, B.; Ji, G. W.; Sun, H. L.; Hu, J. B.; Liang, Z. F.; Gao, X. Y.; Li, H. Y.; Li, Z. S.; Song, B.; et al. On-surface manipulation of atom substitution between cobalt phthalocyanine and the Cu(111) substrate. *RSC Adv.* **2017**, *7*, 13827−13835.
(16) Michaudet, L.; Fasseur, D.; Guilard, R.; Ou, Z.; Kadish, K. M.; Dahaoui, S.; Lecomte, C. J. Synthesis, Characterization and Electrochemistry of Bismuth Porphyrins: X-ray Crystal Structure of (OEP)Bi(SO_3CF_3). *J. Porphyrins Phthalocyanines* **2000**, *04*, 261−270.
(17) Barbour, T.; Belcher, W. J.; Brothers, P. J.; Rickard, C. E. F.; Ware, D. C. Preparation of Group 15 (phosphorus, antimony, and bismuth) Complexes of Meso-tetra-p-tolylporphyrin (TTP) and X-ray Crystal Structure of [Sb(TTP)($OCH(CH_3)_2$)$_2$]Cl. *Inorg. Chem.* **1992**, *31*, 746−754.
(18) Reith, L. M.; Stiftinger, M.; Monkowius, U.; Knör, G.; Schoefberger, W. Synthesis and Characterization of a Stable Bismuth(III) A3-corrole. *Inorg. Chem.* **2011**, *50*, 6788−6797.
(19) Hancock, R. D.; Cukrowski, I.; Baloyi, J.; Mashishi, J. The Affinity of Bismuth(III) for Nitrogen-donor Ligands. *J. Chem. Soc., Dalton Trans.* **1993**, *19*, 2895−2899.
(20) Balieu, S.; Halime, Z.; Lachkar, M.; Boitrel, B. Bismuth Insertion in Functionalized Porphyrins: Influence of the Structure Delivering Substituted Malonic Acid Groups. *J. Porphyrins Phthalocyanines* **2008**, *12*, 1223−1231.
(21) He, B. C.; Tian, G.; Gou, J.; Liu, B. X.; Shen, K. C.; Tian, Q. W.; Yu, Z. Q.; Song, F.; Xie, H. P.; Gao, Y. L.; et al. Structural and Electronic Properties of Atomically Thin Bismuth on Au (111). *Surf. Sci.* **2019**, *679*, 147−153.
(22) Song, F.; Wells, J. W.; Jiang, Z.; Saxegaard, M.; Wahlström, E. Low-Temperature Growth of Bismuth Thin Films with (111) Facet on Highly Oriented Pyrolytic Graphite. *ACS Appl. Mater. Interfaces* **2015**, *7*, 8525−8532.
(23) Scott, S. A.; Kral, M. V.; Brown, S. A. A Crystallographic Orientation Transition and Early Stage Growth Characteristics of Thin Bi Films on HOPG. *Surf. Sci.* **2005**, *587*, 175−184.
(24) Sun, H. L.; Liang, Z. F.; Shen, K. C.; Luo, M.; Hu, J. B.; Huang, H.; Zhu, Z. Y.; Li, Z. J.; Jiang, Z.; Song, F. Fabrication of $NiSe_2$ by Direct Selenylation of a Nickel Surface. *Appl. Surf. Sci.* **2018**, *428*, 623−629.
(25) Perdew, J. P.; Chevary, J. A.; Vosko, S. H.; Jackson, K. A.; Pederson, M. R.; Singh, D. J.; Fiolhais, C. Atoms, Molecules, Solids, and Surfaces: Applications of the Generalized Gradient Approximation for Exchange and Correlation. *Phys. Rev. B: Condens. Matter Mater. Phys.* **1992**, *46*, 6671−6687.
(26) Blöchl, P. E. Projector Augmented-wave Method. *Phys. Rev. B: Condens. Matter Mater. Phys.* **1994**, *50*, 17953−17979.
(27) Kresse, G.; Joubert, D. From Ultrasoft Pseudopotentials to the Projector Augmented-wave Method. *Phys. Rev. B: Condens. Matter Mater. Phys.* **1999**, *59*, 1758−1775.
(28) Henkelman, G.; Uberuaga, B. P.; Jónsson, H. A Climbing Image Nudged Elastic Band Method for Finding Saddle Points and Minimum Energy Paths. *J. Chem. Phys.* **2000**, *113*, 9901−9904.
(29) Chen, M.; Röckert, M.; Xiao, J.; Drescher, H. J.; Steinrück, H. P.; Lytken, O.; Gottfried, J. M. Coordination Reactions and Layer Exchange Processes at a Buried Metal−Organic Interface. *J. Phys. Chem. C* **2014**, *118*, 8501−8507.
(30) Macquet, J. P.; Millard, M. M.; Theophanides, T. X-ray Photoelectron Spectroscopy of Porphyrins. *J. Am. Chem. Soc.* **1978**, *100*, 4741−4746.
(31) Bai, Y.; Buchner, F.; Wendahl, M. T.; Kellner, I.; Bayer, A.; Steinruck, H. P.; Marbach, H.; Gottfried, J. M. Direct Metalation of a Phthalocyanine Monolayer on Ag(111) with Co-adsorbed Iron Atoms. *J. Phys. Chem. C* **2008**, *112*, 6087−6092.
(32) Niwa, Y.; Kobayashi, H.; Tsuchiya, T. X-ray Photoelectron Spectroscopy of Tetraphenylporphin and Phthalocyanine. *J. Chem. Phys.* **1974**, *60*, 799−807.
(33) Eguchi, K.; Nakagawa, T.; Takagi, Y.; Yokoyama, T. Direct Synthesis of Vanadium Phthalocyanine and Its Electronic and Magnetic States in Monolayers and Multilayers on Ag(111). *J. Phys. Chem. C* **2015**, *119*, 9805−9815.
(34) Buchner, F.; Flechtner, K.; Bai, Y.; Zillner, E.; Kellner, I.; Steinruck, H. P.; Marbach, H.; Gottfried, J. M. Coordination of Iron Atoms by Tetraphenylporphyrin Monolayers and Multilayers on Ag(111) and Formation of Iron-Tetraphenylporphyrin. *J. Phys. Chem. C* **2008**, *112*, 15458−15465.
(35) Mugarza, A.; Robles, R.; Krull, C.; Korytar, R.; Lorente, N.; Gambardella, P. Electronic and Magnetic Properties of Molecule-metal Interfaces: Transition Metal Phthalocyanines Adsorbed on Ag(100). *Phys. Rev. B: Condens. Matter Mater. Phys.* **2012**, *85*, 1279−1284.
(36) Shubina, T. E.; Marbach, H.; Flechtner, K.; Kretschmann, A.; Jux, N.; Buchner, F.; Steinrück, H.-P.; Clark, T.; Gottfried, J. M. Principle and Mechanism of Direct Porphyrin Metalation: Joint Experimental and Theoretical Investigation. *J. Am. Chem. Soc.* **2007**, *129*, 9476−9483.
(37) Gottfried, J. M. Surface Chemistry of Porphyrins and Phthalocyanines. *Surf. Sci. Rep.* **2015**, *70*, 259−379.
(38) Hofmann, P. The Surfaces of Bismuth: Structural and Electronic Properties. *Prog. Surf. Sci.* **2006**, *81*, 191−245.
(39) Baran, J. D.; Larsson, A. J. Theoretical Insights into Adsorption of Cobalt Phthalocyanine on Ag(111): A Combination of Chemical and van der Waals Bonding. *J. Phys. Chem. C* **2013**, *117*, 23887−23898.
(40) Baran, J. D.; Larsson, J. A.; Woolley, R. A. J.; Cong, Y.; Moriarty, P. J.; Cafolla, A. A.; Schulte, K.; Dhanak, V. R. Theoretical and Experimental Comparison of SnPc, PbPc and CoPc Adsorption

https://dx.doi.org/10.1021/acs.jpcc.0c00895
J. Phys. Chem. C 2020, 124, 8247−8256

on Ag(111). *Phys. Rev. B: Condens. Matter Mater. Phys.* **2010**, *81*, 075413.

https://dx.doi.org/10.1021/acs.jpcc.0c00895
J. Phys. Chem. C 2020, 124, 8247−8256